(Received 28 October 2025, Accepted 1 December 2025, Scheduled 2 January 2026)

Enhanced Impedance Matching in Microstrip Grid Array Antenna Using Differential-Shifted Feeding and Parasitic Patches

Rajamohan Varun Prakash*, Jeyagobi Logeswaran, Atham Mohamed Mahin Ayas, and Pandurangan Sridhar

Department of ECE, Mepco Schlenk Engineering College, Sivakasi, Tamilnadu, India

ABSTRACT: This paper aims to design and analyze a tri-band Differential Shifted-Feed Microstrip Grid Array Antenna (DSF-MGAA) with eight parasitic elements to achieve better return loss and isolation characteristics and improved antenna gain at various frequency ranges in the Golden band, X-band, and Ku band. The nonuniform grid element is excited through two 180-degree out-of-phase signal-carrying feed lines with the LC matching network to provide better impedance matching. The antenna provides a minimum peak return loss of −17.88 dB, −27.13 dB and −26.7 dB at 7 GHz, 9 GHz and 12.2 GHz. Measured results show a good agreement with the simulated results. Parasitic elements incorporated provide a maximum gain of 17.2 dBi. The results confirm that the proposed antenna suits for high-frequency applications such as 6G communication, Space and Defense application, and VSAT (Very Small Aperture Terminal) networks.

1. INTRODUCTION

The need for high-performance antennas has recently grown extremely fast with the development of wireless communications technology and increasing demands for fast, stable data transmission. From satellite transmissions and radar installations to television broadcasting and next-generation 5G networks, contemporary communications depend heavily on efficient antennas [5, 16, 18]. Microstrip antennas have also emerged as an ideal solution for most of these areas because they are low-profile, lightweight, and easy to integrate into electronic systems [5, 14, 19, 20]. However, despite their pervasiveness, microstrip antennas often struggle with one main concern — impedance matching at high frequencies. If impedance is not matched, it can lead to unwanted reflections of the signal, and hence there will be a loss of signal and a decrease in system performance.

To overcome this, scientists have sought new designs beyond the conventional microstrip patch. One such design is the DSF-MGAA with an LC matching network. This is a new design in employing a nonuniform grid array, which enhances impedance matching and minimizes signal loss — both of which are important for high-frequency applications [1, 2, 6]. In addition to DSF-MGAA designs, grid-array structures have also been explored for switched-beam and beam-steering mm-wave applications, and also it may enhance gain and bandwidth using a nonuniform grid and multiple parasitic patches [22–24]. The differential feeding method also provides improved symmetry and isolation, which is particularly useful in complicated systems where interference and coupling can be troublesome [1, 9, 13, 20, 21]. Another important development comes by the use of parasitic elements — small, correctly placed patches that do not directly couple to the feed but influence the antenna performance. The elements can be utilized to control and steer radiated energy, to enhance gain and directivity without significant enlargement in the size of the antenna [3, 4, 15]. Although the aforementioned approach provides a better response, further impedance matching may be achieved by including an LC matching network. Parasitic element combined grid array structures have demonstrated very significant enhancements in bandwidth as well as in total efficiency [2, 3, 14]. For instance, recent work has shown how nonuniform grid arrays can facilitate wideband filtering antennas with good performance in compact design [2, 8]. Parasitic patches have also been found by other researchers to boost MIMO antenna systems significantly, improving isolation and gain [3]. Further studies have shown the utility of inductive grid-array metasurfaces for creating low-profile, electrically small, and wideband antennas [7, 8, 11, 12], while dual-band differentially-fed filtennas have demonstrated high selectivity and low cross-polarization ideal for multi-band applications [9, 10, 17].

This paper presents the design technique and performance of an eight parasitic patch DSF-MGAA, designed specifically to operate in the Ku-band frequency range. The antenna has a significant gain of 17.2 dBi, which is a testament to its suitability for use in several high-frequency applications. The following

* Corresponding author: Rajamohan Varun Prakash (varunprakash.r@mepcoeng.ac.in).

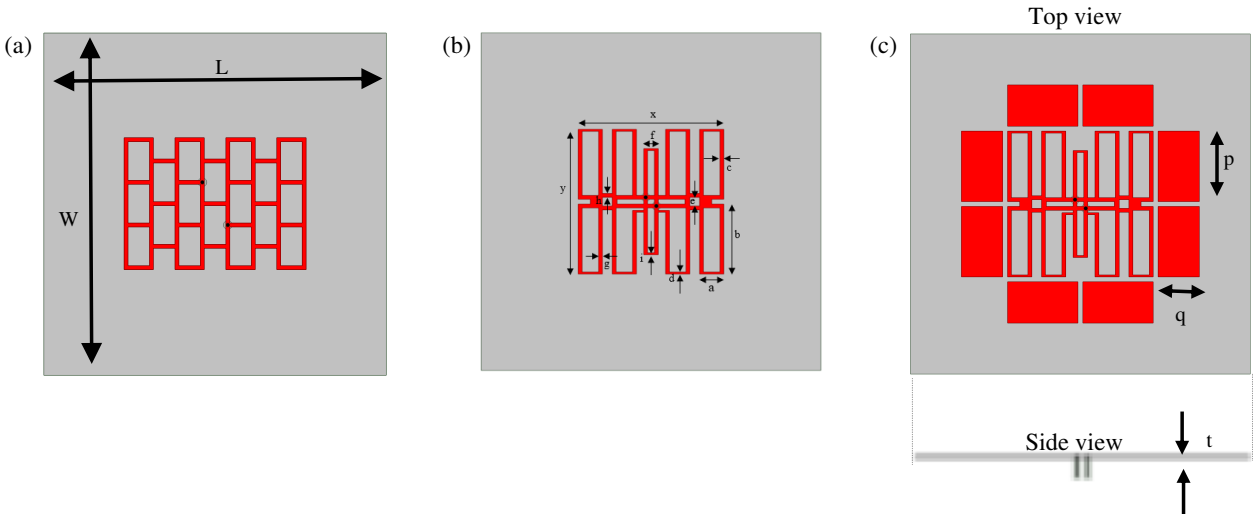

FIGURE 1. Antenna configuration and dimensions of (a) uniform-MGAA, (b) nonuniform-MGAA, and (c) nonuniform-MGAA with eight parasitic patches.

sections will detail the design methodology, simulation results, and practical implications of the DSF-MGAA.

2. ANTENNA DESIGN AND OPERATING PRINCIPLE

2.1. Configuration and Principle of Operation

Figure 1(a) presents the structural layout of the uniform Microstrip Grid Array Antenna (MGAA), implemented on a grounded RT/duroid 5880 substrate characterized by a dielectric constant of 2.2, a loss tangent of 0.0009, and a substrate length and width denoted by L & W. The uniform MGAA is designed initially. By modifying the dimensions of the uniform MGAA, it can be transformed into a nonuniform MGAA as shown in Fig. 1(b). The detailed dimensions of the proposed nonuniform MGAA is given in Table 1. Additionally, a differential shifted feeding scheme is implemented, along with eight parasitic patches, as depicted in Fig. 1(c).

TABLE 1. Antenna parameters and dimensions (in mm)

a	b	c	d	e	f	g	h
5	14.5	0.8	0.4	1.8	3	0.8	0.8
i	L	p	q	W	x	y	t
0.4	70	14.5	8.5	70	30	30	0.787

2.2. Design of Uniform-MGAA

The uniform MGAA consists of 25 short segments, each with a length d_u and a width w_u, as well as 24 long segments that have a length d_v and a width w_v, Fig. 1(a). To simplify the design, the antennas utilize two 50-ohm coaxial connectors for excitation. Nevertheless, other feeding techniques can also be applied.

The uniform MGAA showcases multi-band activity, with -28.8290 dB for return loss (S_{11}) at 7.55 GHz and -25.6259 dB at 11.35 GHz,as shown in Fig. 2(a). Along with this, the respective values of S_{22} at 7.55 GHz and 11.35 GHz are -30.330 dB and -23.633 dB, as depicted in Fig. 2(b). Although there is support by the antenna in multiple frequency bands, these two frequencies show better performance.

Figure 3 indicates that the antenna also provides port-to-port isolation at different frequency bands. From Figure 3, it is clear that isolation values of -25.1588 dB, -27.9449 dB, and -24.6855 dB are achieved at 9.20 GHz, 14.05 GHz, and 13.35 GHz, respectively.

Figure 4 illustrates the three-dimensional gain radiation pattern of the antenna described. The antenna's peak gain is 4.7 dB, and the radiation concentrates predominantly in the upper hemisphere, which indicates a directional radiation pattern.

2.3. Design of Nonuniform MGAA

Nonuniform MGAA structure: The grid units are made to transition from uniform to nonuniform spacings across the array. The center elements are lengthened and the edge ones shortened, introducing structural asymmetry that individualizes resonant frequencies, broadens the overall bandwidth, and enhances inter-element isolation — hence enhancing multi-band and MIMO performance. The feed points are also redesigned to further enhance the antenna response.

Figure 5(a) indicates that the antenna demonstrates effective operation across various frequency bands with high-quality resonant dips at 11.99 GHz (-28.58 dB), 12.25 GHz (-28.13 dB), and 13.53 GHz (-25.63 dB). The simulated S_{22} parameter plot demonstrates clear resonant dips at 8.98 GHz, 11.90 GHz, and 14.11 GHz with return loss measures of -20.40 dB, -28.33 dB, and -22.80 dB, respectively, as illustrated in Fig. 5(b). Such low S_{11} and S_{22} values demonstrate effective power transfer and minimal signal reflection.

Figure 6 indicates that the antenna has good port isolation for a variety of frequency bands. More surprisingly, isolation values of -23.7271 dB at 9.6188 GHz, -30.5441 dB at 13.8225 GHz, and -24.1378 dB at 16.1025 GHz are obtained.

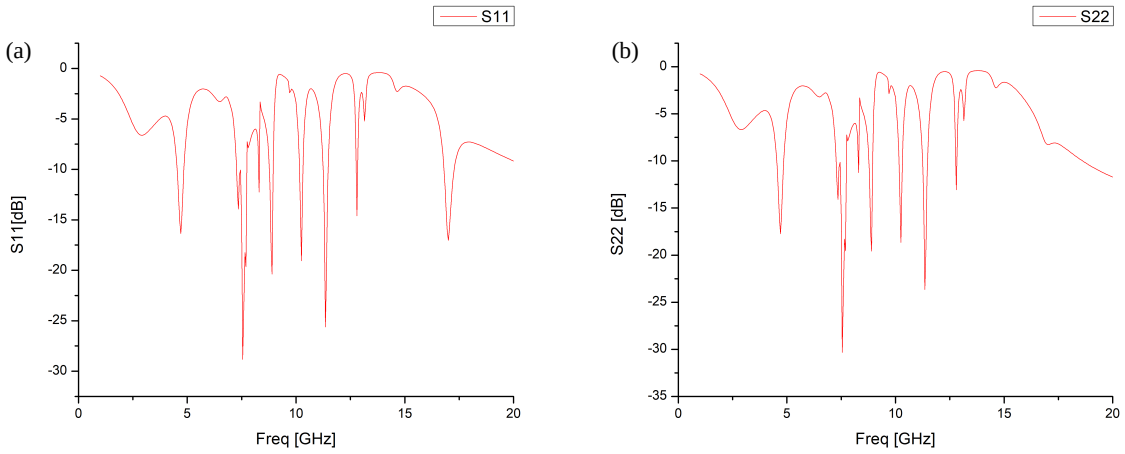

FIGURE 2. Simulated reflection coefficients. (a) S_{11} and (b) S_{22} of uniform-MGAA.

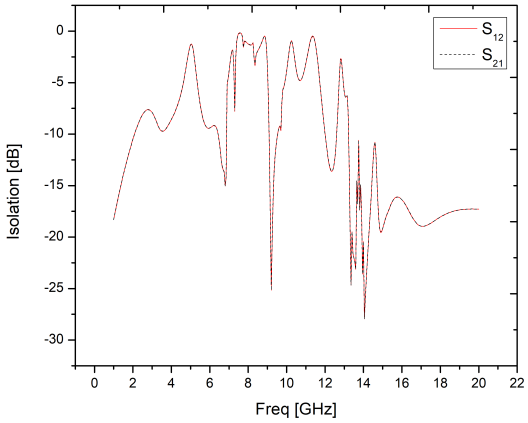

FIGURE 3. Simulated isolation (S_{12} and S_{21}) of uniform-MGAA.

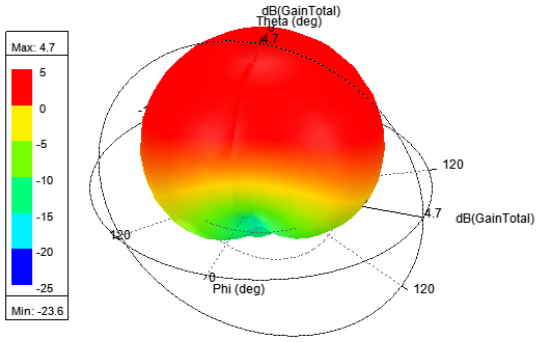

FIGURE 4. 3D gain radiation pattern.

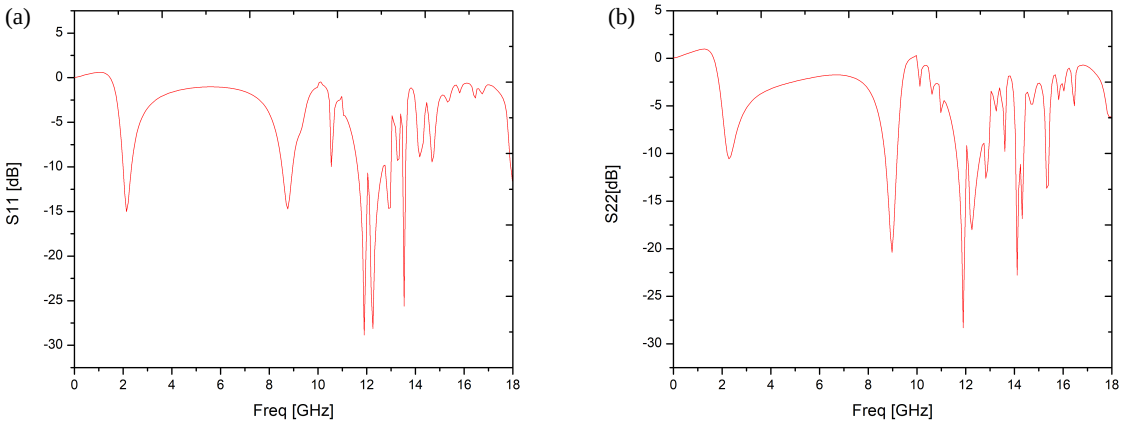

FIGURE 5. Simulated S-parameter. (a) S_{11} & (b) S_{22} curve of the nonuniform MGAA structure.

2.4. Design of DSF Nonuniform MGAA

To achieve better impedance compatibility and overall performance of the nonuniform MGAA, a differential shifted feeding (DSF) mechanism and eight parasitic patches are utilized. The DSF is used to provide a 180° phase difference across bands at the same time, essentially enhancing impedance matching and greatly increasing bandwidth, especially around the frequency band of 14 GHz. Additionally, the eight parasitic elements of size 14.5 mm in length and 8.5 mm in width are strategically placed within the structure to improve electromagnetic coupling and surface current distribution. These enhancements all lead to greater antenna gain, improved radiation efficiency, and greater applicability in high-frequency operations.

A co-simulation environment was established in ANSYS Electronics Desktop by combining High Frequency Structure Simulator (HFSS) with Circuit Designer to simulate the DSF-

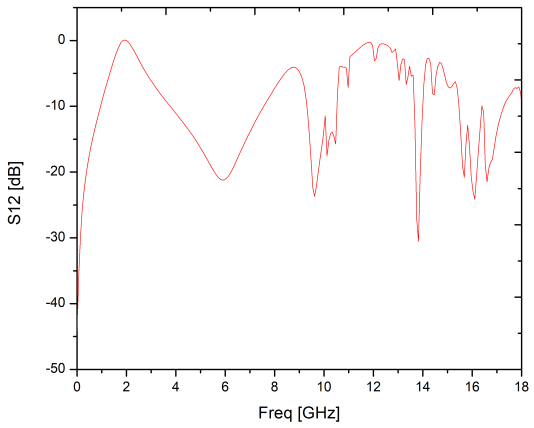

FIGURE 6. Simulated isolation S_{12} of non uniform MGAA.

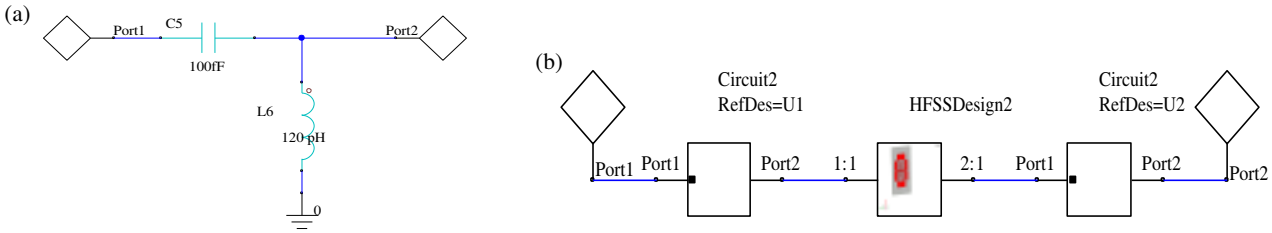

FIGURE 7. (a) LC network and (b) shows the LC network connected to both input ports of the MGAA to symmetrically improve impedance matching and support differential feeding.

based nonuniform Microstrip Grid Array Antenna (MGAA). In this setup, an RF signal is provided at the input port and passed through a circuit block (Circuit2-U1), which is constructed as an LC matching network, as shown in Fig. 7(a). This circuit is connected to the HFSSDesign2 block, which simulates the electromagnetic (EM) response of the antenna structure, including differential feeding. The output of the HFSS block is then fed through a second circuit block (Circuit2-U2) and exits at the output port, as shown in Fig. 7(b). This combined simulation approach enables complete performance analysis through circuit-level and full-wave EM simulations in a single step, enabling precise characterization of return loss, isolation, and overall antenna performance.

The comparison of the the nonuniform MGAA without and with differential shifted feeding antennas is illustrated in Figure 8, and better bandwidth and performance are clearly indicated using the given method.

The comparison illustrates the efficiency of differential shifted feeding (DSF) in improving antenna performance. Without DSF, the return loss at 14.0474 GHz is -11.0921 dB, which represents moderate impedance matching, with a simulated -10 dB impedance bandwidth of 13.74 to 14.0474 GHz. With DSF, several resonant dips are seen, such as -22.1140 dB at 8.8271 GHz and a much deeper -38.0427 dB at 14.0872 GHz. The corresponding -10 dB impedance bandwidth is from 13.54 to 14.45 GHz, as indicated in Fig. 8(a). This significant improvement at around 14 GHz attests to improved impedance matching and a broader operational bandwidth, proving the advantages of the DSF method.

Figure 8(b) indicates that without DSF, the isolation at 14 GHz is -4.2774 dB, while with DSF, it improves considerably to -20.2514 dB at 14.0872 GHz, reflecting less mutual coupling between ports. By suppressing unwanted coupling effectively, the DSF method provides improved signal integrity and increased isolation.

Compared to the conventional uniform grid structure, the proposed nonuniform grid structure has multiple peak minimum reflection coefficient values, as shown in Fig. 9. Without DSF, the antenna exhibits a peak gain of 10.6 dB and a less focused, wider radiation pattern. When DSF is introduced, the gain increases to 17.2 dB and is more focused in its radiation, as shown in Figs. 10 (a) & (b). This demonstrates that the parasitic elements and the DSF are important in increasing gain and directionality factor of the antenna. DSF may alter the amplitude and phase distribution of the radiated fields over the aperture. By appropriately positioning and dimensioning the DSF elements to half a wavelength, the fields scattered from the DSF add constructively in the main radiation direction, which narrows the main beam and increases the effective aperture, thereby enhancing gain and directivity.

In conjunction with DSF implementation, an LC matching network is utilized in order to further improve impedance matching, as indicated in Fig. 7(b). This pairing brings the antenna impedance closer to the conventional 50 Ω standard, thus increasing power transfer and overall radiation performance. The efficiency of this method is illustrated by comparing the

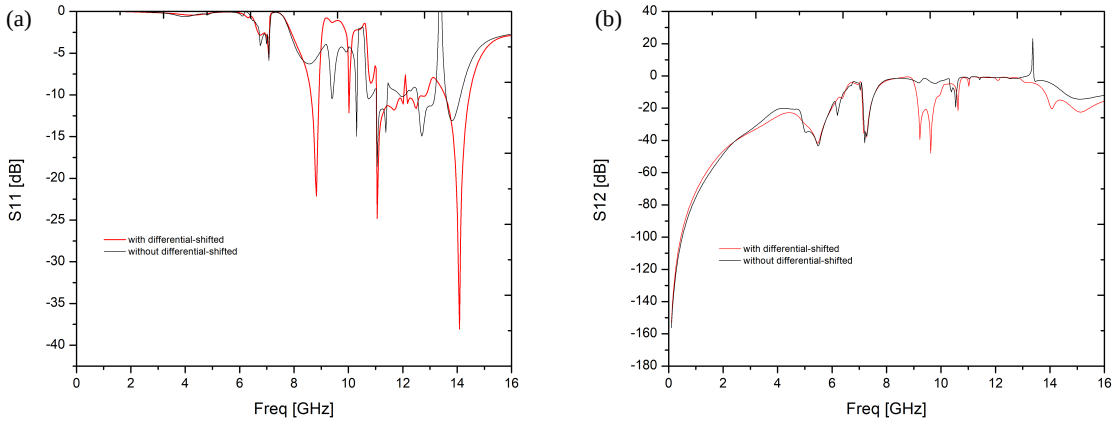

FIGURE 8. Comparison of the nonuniform MGAA with and without differential shifted feeding (DSF). (a) Simulated reflection coefficient (S_{11}), and (b) isolation (S_{12}).

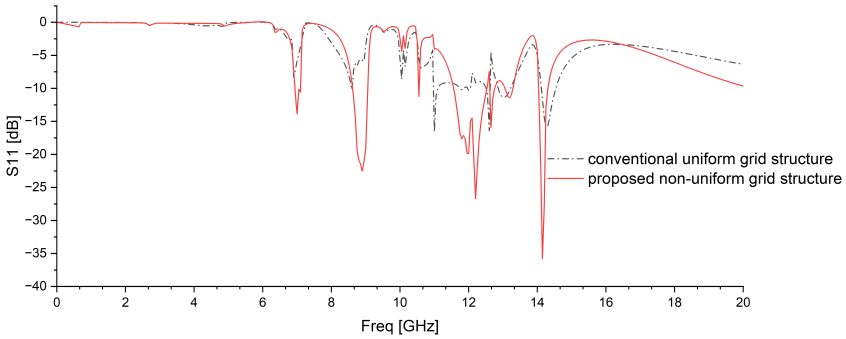

FIGURE 9. Comparison of the simulated reflection coefficient (S_{11}) of the conventional uniform vs proposed nonuniform MGAA.

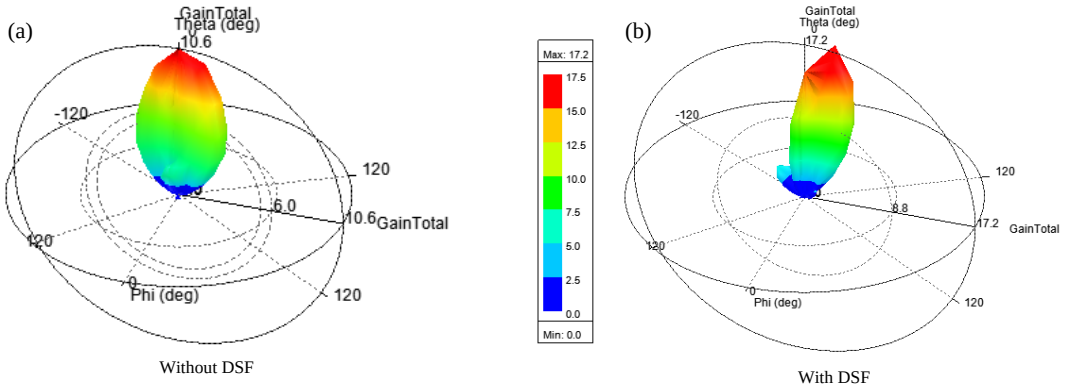

FIGURE 10. (a) and (b) illustrate the 3D gain patterns of the antenna in the presence and absence of DSF.

input impedance (Z-parameter) at 14 GHz: without DSF, the impedance is 17.0482 Ω, which means poor matching, while with DSF, it becomes much better at 53.5539 Ω — much closer to the target value — leading to more efficient operation at this frequency.

The directivity comparison between the two configurations at 14 GHz ($\Phi = 180$) as illustrated in Fig. 11.

Without DSF, the antenna has reduced peak directivity and increased side lobes, which means that it is less efficient in radiation in the target direction. On the other hand, with DSF, increased main lobe and suppressed side lobes are noted, leading to enhanced beam steering performance at 14 GHz.

The present distribution of the DSF-MGAA, as presented in Fig. 12, shows that the most intense electric field levels — and by extension of the highest surface currents — are at the central feed lines and major radiating elements, shown by the red and orange areas. These are the main radiation sources because of the differential feeding approach. The parasitic patches surrounding it, with moderate field intensities (yellow to green), display induced currents due to mutual coupling, which contribute to enhancing radiation pattern control and overall gain.

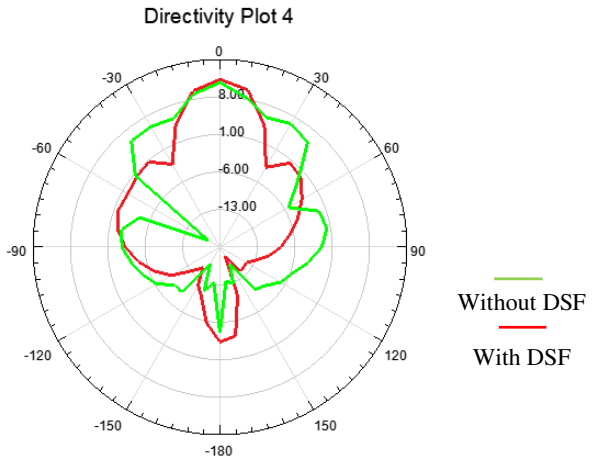

FIGURE 11. Directivity.

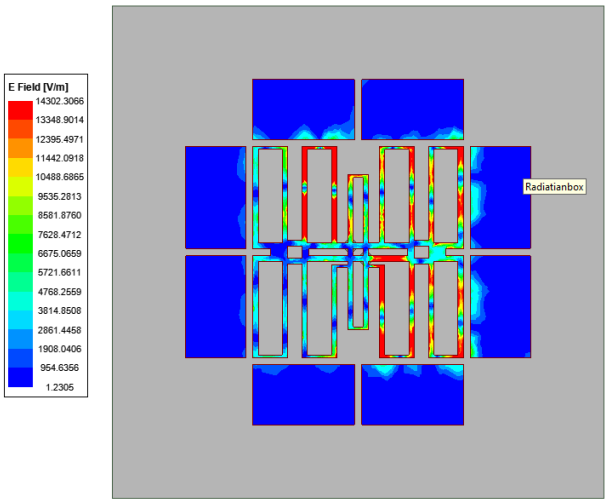

FIGURE 12. E-field representation.

Lower field intensity areas (blue) reflect the fringing fields responsible for bandwidth enhancement. The measured symmetrical current distribution confirms the balanced operation of the array and highlights the successful interaction between the driven and parasitic elements that are responsible for the enhanced performance of the antenna.

3. MEASUREMENTS AND RESULTS

This part presents a comparative investigation of the simulated and measured results for the nonuniform Microstrip Grid Array Antenna (MGAA) structure with Differential Shifted Feeding (DSF) and eight parasitic elements. Fig. 13 shows photographs of the fabricated antenna prototype. The antenna testing setup is depicted in Fig. 14, where a Vector Network Analyzer (VNA) is used to test important performance parameters, such as return loss, isolation, and Voltage Standing Wave Ratio (VSWR). The antenna is connected through SMA connectors, and differential feeding is achieved with paired cables. The VNA measures the parameters across a frequency band of 1–16 GHz and facilitating the evaluation of impedance matching and the overall operating performance of the antenna.

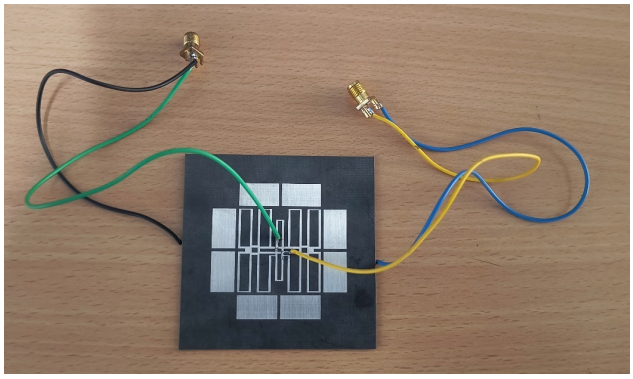

FIGURE 13. Photo of fabricated antenna.

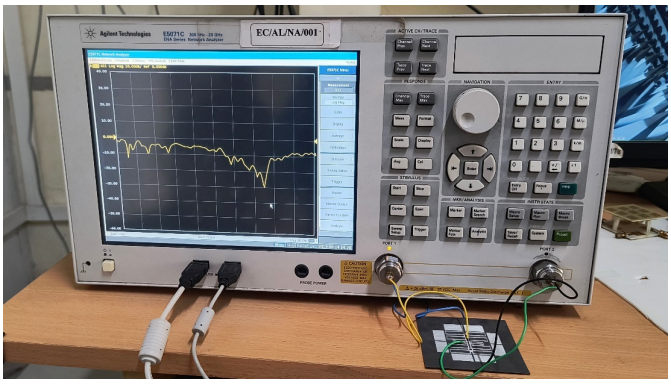

FIGURE 14. Testing of antenna in Vector Network Analyzer.

3.1. Reflection Coefficient

Simulated and experimental results for return loss (S_{11}) characteristics of the suggested DSF-based nonuniform Microstrip Grid Array Antenna (MGAA) are shown in Fig. 15(a). The antenna shows broadband operation over the frequency band 2–16 GHz. In the simulated response, clear-cut resonant dips are seen at 8.83 GHz (−22.11 dB), 11.07 GHz (−24.82 dB), and 14.09 GHz (−38.04 dB), with the −10 dB impedance bandwidth covering from 13.54 GHz to 14.45 GHz, which reveals excellent impedance matching. The experimental results also reflect strong resonance properties, with return loss values of −28.13 dB at 13.07 GHz and −26.83 dB at 13.58 GHz. Its corresponding −10 dB bandwidth is around 11 GHz to 15.4 GHz, which proves its broadband nature and validates the efficient radiation and impedance matching of the antenna.

The S_{22} parameter, depicted in Fig. 15(b), indicates return loss at port 2 in both simulated and measured responses. The simulated curve has resonating dips at 8.83 GHz (−28.12 dB), 10.06 GHz (−23.31 dB), 12.97 GHz (−19.84 dB), and 14.25 GHz (−27.18 dB). The measured ones are also substantially close to them with return loss of −28.77 dB at 13.67 GHz and −22.02 dB at 14.09 GHz, ascertaining good port isolation and broadband characteristics of the antenna.

3.2. Isolation

The S_{12} parameter plot, as given in Fig. 16, indicates the isolation among the feed points of the MGAA within the 2–16 GHz

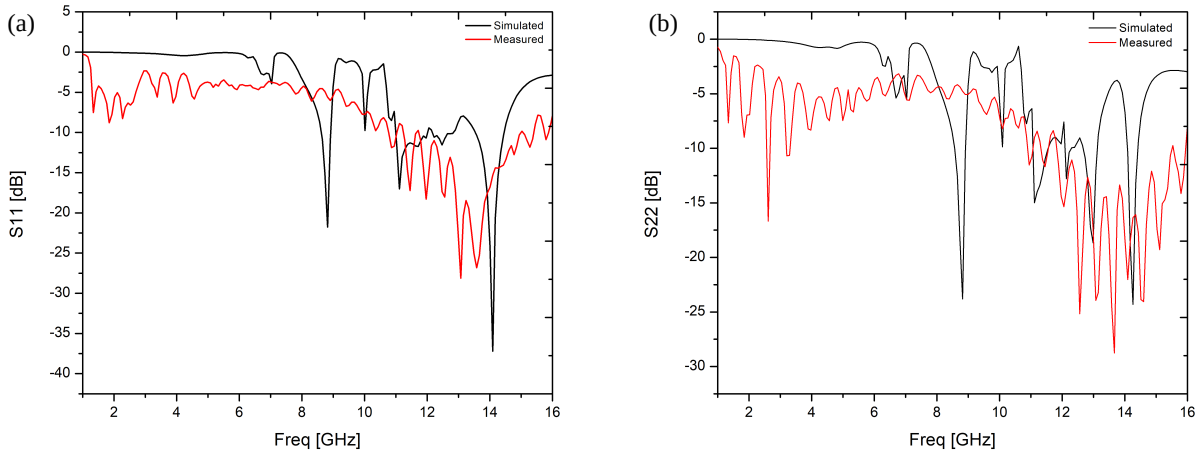

FIGURE 15. Simulated and measured. (a) Reflection coefficients (S_{11}) & (b) reflection coefficients (S_{22}) of the DSF-based nonuniform MGAA.

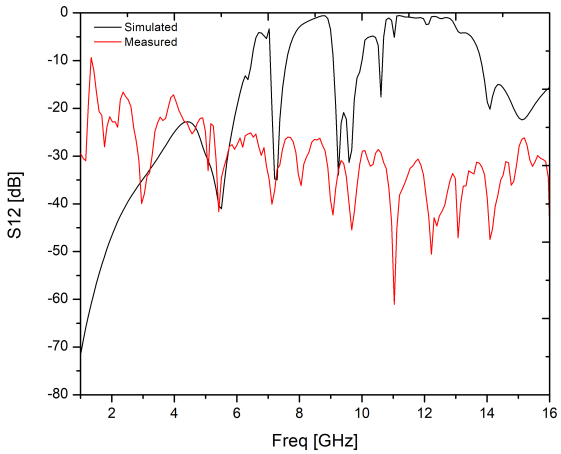

FIGURE 16. Simulated and experimental isolations.

frequency range. From the simulated response, the antenna realizes an isolation of -20.25 dB at 14.09 GHz and -23.37 dB at 15.5 GHz, showing moderate suppression of mutual coupling among the ports. Conversely, the measured values show considerably improved isolation, with -47.44 dB at 14.09 GHz and -27.68 dB at 15.5 GHz. This high measured port isolation is an indication of good decoupling, which is a key requirement for MIMO systems to provide low inter-port interference and better diversity performance.

3.3. VSWR

The simulated VSWR at port 1 of the suggested antenna is less than the traditional limit of 2 over a very broad frequency range, reflecting good impedance matching and minimal mismatch losses, especially at higher frequencies. The values show minor variation but remain within acceptable limits over the 6–16 GHz range. The measured VSWR also exhibits this pattern, with values remaining near 1 over the same frequency range, as shown in Fig. 17(a). This indicates very effective power transfer and very good impedance matching in real-world applications.

The VSWR plot of port 2, Fig. 17(b), shows both simulated and measured results over the 1–16 GHz frequency range. The simulated VSWR is as low as 1.87, showing good impedance matching and acceptable reflection levels, especially in the higher frequency range. The VSWR value also measured from the realized antenna improves the simulated response further to a lowest value of 1.8, thus verifying successful impedance matching and effective power transfer under real conditions. The observed performance validates the antenna's effectiveness for high-frequency applications, covering Ku-band very effectively.

3.4. Comparison and Discussion

Table 2 gives a comparative overview of the major performance parameters of the proposed DSF-MGAA from both simulated and experimental data. The simulated frequency range is between 8 GHz and 16 GHz, whereas the measured frequency range is slightly shifted, ranging from 11 GHz to 16 GHz. The simulated response shows a minimum return loss of -38.04 dB, while the measured return loss is -28.13 dB, both reflecting superb impedance matching. The simulated VSWR is 1.86, with a better measured value of 1.31, implying improved efficiency in power transfer in actual implementation. Additionally, the simulated port isolation is -20.25 dB, while it greatly improves to -47.44 dB in the measured data, ascertaining robust port decoupling and establishing the antenna as appropriate for MIMO applications.

The difference between measurement and simulation return loss variability is primarily as a result of PCB fabrication tolerance and solder flaws of the connectors, which would lead to shifts in frequency as well as increased signal losses.

TABLE 2. Simulation and measurement comparisons of DSF MGAA.

Parameters	Simulated result	Measured result
Operating Frequency	8 GHz–16 GHz	11 GHz–16 GHz
Return Loss	-38.0427 dB	-28.127 dB
VSWR	1.86	1.31
Isolation Loss	-20.2514 dB	-47.4359 dB

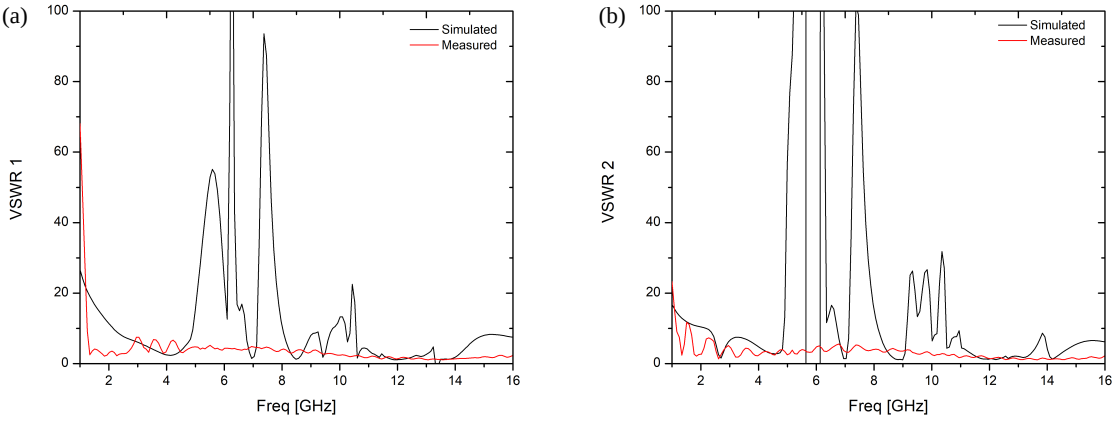

FIGURE 17. Simulated and measured (a) VSWR of port 1 and (b) VSWR of port 2 of the antenna.

TABLE 3. Comparisons of DSF MGAA for uniform vs nonuniform grid structures.

Reference	Antenna structure	Operating frequency (GHz)	BW (%)	Gain (dBi)
[1]	Uniform Grid/ two parasitic patch	3.7/28.5	3.4/4.5	8.98/ 19.2
This Work	Non uniform/ eight parasitic patch	11 GHz–16 GHz	28.12	17.2

With respect to [1], in which a uniform grid is utilized with two parasitic patches with operation at two narrow bands (3.7 GHz with bandwidth 3.4% and 28.5 GHz with bandwidth 4.5%) and provides gains of 8.98 dBi and 19.2 dBi, respectively. In the proposed work, nonuniform spacing may be chosen so that some cells resonate or couple more strongly at one band and others at the second band, and similarly at the third band, hence, aiding the tri-band operation, and more parasitic patches provide additional degrees of freedom in lengths and positions to generate multiple closely spaced resonances. Distributed parasitics help control the phase front and aperture illumination more finely, leading to higher gain. This yields a wider bandwidth of 28.12% and high gain of 17.2 dBi over the band, and this comparison is illustrated in Table 3. Improved impedance matching, wider bandwidth, and high-gain stability are achieved by the new configuration and larger parasitic element count, which improve the design for wideband and high-frequency operations.

4. CONCLUSION

The proposed antenna designed from a uniform to a nonuniform Microstrip Grid Array Antenna (MGAA) is achieved through different spacings and positions of the elements, such that there would be more flexibility in controlling high-frequency resonant properties. The addition of Differential Shifted Feeding (DSF) greatly enhances performance, with a simulated return loss of -38.04 dB and isolation of -20.25 dB at 14.0872 GHz, reflecting very good impedance matching and lower mutual coupling. In measurement, the antenna shows a return loss of -28.77 dB, isolation of -47.44 dB, and VSWR of 1.31, ascertaining solid real-world performance. The measured band ranges from 11 GHz to 15.5 GHz, with a wide frequency band useful in many high-frequency applications. The insertion of eight parasitic elements further enhances the design by increasing the gain to 17.2 dB and minimizing beamwidth, thereby increasing directivity and suppressing side lobe. In addition, an LC matching network is utilized to achieve impedance matching close to 50-ohm. Collectively, these enhancements validate the antenna's applicability in high-frequency systems, ensuring high gain, wide bandwidth, improved impedance matching, and improved isolation characteristics.

ACKNOWLEDGEMENT

The authors would like to express their sincere gratitude to the Centre for Excellence in RF Circuit and Antenna Design, Department of Electronics and Communication Engineering, Mepco Schlenk Engineering College (Autonomous), Sivakasi, India, for extending support and access to the Vector Network Analyzer and Anechoic Chamber facility (800 MHz–20 GHz) for antenna characterization and measurements.

REFERENCES

[1] Xu, G., H.-L. Peng, Z. Shao, L. Zhou, Y. Zhang, and W.-Y. Yin, "Dual-band differential shifted-feed microstrip grid array antenna with two parasitic patches," *IEEE Transactions on Antennas and Propagation*, Vol. 68, No. 3, 2434–2439, Mar. 2020.

[2] Lang, Y.-L., D. Yi, and M.-C. Tang, "Single-layer and wideband filtering antenna with small footprint based on non-uniform grid array," *IEEE Transactions on Antennas and Propagation*, Vol. 72, No. 9, 7287–7292, Sep. 2024.

[3] Zhao, B., M. Tang, Z. Shao, Y. Zhang, and J. Mao, "Design of broadband compact grid array antennas using gradient slow-wave structures," *IEEE Antennas and Wireless Propagation Letters*, Vol. 21, No. 3, 620–624, Mar. 2022.

[4] Tran, H. H. and N. Nguyen-Trong, "Performance enhancement of MIMO patch antenna using parasitic elements," *IEEE Access*, Vol. 9, 30 011–30 016, Feb. 2021.

[5] Chen, X., J. Wang, and L. Chang, "Extremely low-profile dual-band microstrip patch antenna using electric coupling for 5G mobile terminal applications," *IEEE Transactions on Antennas and Propagation*, Vol. 71, No. 2, 1895–1900, Feb. 2023.

[6] Ren, J., M. Zuo, B. Zhang, X. Du, Z. Chen, Y. Liu, and Y. Z. Yin, "Large frequency ratio Vivaldi antenna system with low-frequency gain enhancement utilizing dual-function taper slot," *IEEE Transactions on Antennas and Propagation*, Vol. 70, No. 6, 4854–4859, Jun. 2022.

[7] Chen, C., "A wideband coplanar L-probe-fed slot-loaded rectangular filtering microstrip patch antenna with high selectivity," *IEEE Antennas and Wireless Propagation Letters*, Vol. 21, No. 6, 1134–1138, Jun. 2022.

[8] Guo, Y. Q., Y. M. Pan, S. Y. Zheng, and K. Lu, "A singly-fed dual-band microstrip antenna for microwave and millimeter-wave applications in 5G wireless communication," *IEEE Transactions on Vehicular Technology*, Vol. 70, No. 6, 5419–5430, Jun. 2021.

[9] Xu, G., L.-X. Yang, Z.-X. Huang, W. Wang, H.-L. Peng, Y. Zhang, and W.-Y. Yin, "Microstrip grid and patch-based dual-band shared-aperture differentially fed array antenna," *IEEE Antennas and Wireless Propagation Letters*, Vol. 20, No. 6, 1043–1047, Jun. 2021.

[10] Hu, K.-Z., M.-C. Tang, D. Li, Y. Wang, and M. Li, "Design of compact, single-layered substrate integrated waveguide filtenna with parasitic patch," *IEEE Transactions on Antennas and Propagation*, Vol. 68, No. 2, 1134–1139, Feb. 2020.

[11] Lin, Q., M.-C. Tang, X. Chen, D. Yi, M. Li, and R. W. Ziolkowski, "Low-profile, electrically small, ultrawideband antenna enabled with an inductive grid array metasurface," *IEEE Transactions on Antennas and Propagation*, Vol. 70, No. 8, 7152–7157, Aug. 2022.

[12] Lin, Q., M.-C. Tang, M. Li, and R. W. Ziolkowski, "Electrically small, wideband, circularly polarized, inductive grid-array metasurface antenna," *IEEE Transactions on Antennas and Propagation*, Vol. 71, No. 5, 4546–4551, May 2023.

[13] Li, D., M.-C. Tang, Y. Wang, K.-Z. Hu, and R. W. Ziolkowski, "Dual-band, differentially-fed filtenna with wide bandwidth, high selectivity, and low cross-polarization," *IEEE Transactions on Antennas and Propagation*, Vol. 70, No. 6, 4872–4877, Jun. 2022.

[14] Srivastava, S. and N. S. Rajput, "Wide band microstrip patch antenna array with parasitic element for automotive radar applications," in *2022 3rd URSI Atlantic and Asia Pacific Radio Science Meeting (AT-AP-RASC)*, 1–3, Gran Canaria, Spain, 2022.

[15] Wang, M., Y.-H. Ren, X.-Y. Jin, Y.-Y. Wang, H.-D. Wu, and Ke-Li, "Design of a broadband miniaturized microstrip grid array antenna with slow wave transmission lines," in *2022 International Conference on Microwave and Millimeter Wave Technology (ICMMT)*, 1–3, Harbin, China, 2022.

[16] Yang, M., Q. Wu, K. Zheng, S. Zhang, and G. Wei, "Radiation field distribution above sea surface of underwater microstrip antenna array," *IEEE Antennas and Wireless Propagation Letters*, Vol. 23, No. 2, 858–862, Feb. 2024.

[17] Xu, G., L.-X. Yang, Z.-X. Huang, W. Wang, H.-L. Peng, Y. Zhang, and W.-Y. Yin, "Microstrip grid and patch-based dual-band shared-aperture differentially fed array antenna," *IEEE Antennas and Wireless Propagation Letters*, Vol. 20, No. 6, 1043–1047, Jun. 2021.

[18] An, K., P. Sun, Y. Deng, and A. Chen, "A large-scale high-gain transparent grid array antenna for millimeter-wave communication," *IEEE Antennas and Wireless Propagation Letters*, Vol. 23, No. 5, 1598–1602, May 2024.

[19] Arnieri, E., F. Greco, L. Boccia, and G. Amendola, "A reduced size planar grid array antenna for automotive radar sensors," *IEEE Antennas and Wireless Propagation Letters*, Vol. 17, No. 12, 2389–2393, Dec. 2018.

[20] Arrawatia, M., M. S. Baghini, and G. Kumar, "Differential microstrip antenna for RF energy harvesting," *IEEE Transactions on Antennas and Propagation*, Vol. 63, No. 4, 1581–1588, Apr. 2015.

[21] Logeswaran, J. and R. B. Rani, "Design and analysis of miniaturized asymmetric CPW-fed 5.8 GHz antenna for RFID applications," *National Academy Science Letters*, Vol. 47, No. 5, 551–554, 2024.

[22] Nasimuddin, Y. Zhou, and X. Qing, "Millimeter-wave switched-beam grid-array antenna," in *2023 17th European Conference on Antennas and Propagation (EuCAP)*, 1–4, Florence, Italy, 2023.

[23] Nasimuddin, and X. Qing, "Switchable beam steering antenna for Ka-band airborne applications," in *2020 IEEE International Conference on Computational Electromagnetics (ICCEM)*, 201–202, Singapore, 2020.

[24] Sun, M., Nasimuddin, X. Qing, and Z. N. Chen, "Circularly polarized switched beams grid array antenna for mm-Wave systems," in *2019 IEEE Asia-Pacific Microwave Conference (APMC)*, 1598–1600, Singapore, 2019.